Geophys. J. Int. (1999) **138,** 801–808

Determination of the fault plane using a single near-field seismic station with a finite-dimension source model

D. Legrand[1,2] and B. Delouis[3]

[1] *Earthquake Research Institute, University of Tokyo,* 1–1-1 *Yayoi, Bunkyo-ku, Tokyo* 113, *Japan. E-mail: denis@rerere.eri.u-tokyo.ac.jp*
[2] *Maison Franco Japonaise,* 3–9-25 *Ebisu, Shibuya-ku Tokyo* 150–0013, *Japan. E-mail: legrand@mfj.gr.jp*
[3] *ETH, Institut fur Geophysik, Honggerberg,* CH-8093, *Zurich, Switzerland. E-mail: bertrand@seismo.ifg.ethz.ch*

Accepted 1999 May 4. Received 1999 April 10; in original form 1998 December 10

SUMMARY

We explore the possibility of determining the actual fault plane of an earthquake from the inversion of near-source displacement seismograms of one station when a finite-dimension source is used instead of a point source model and when the complete displacement is taken into account, including near-field waves. Tests on synthetic seismograms and real data recorded at local distances show that this is possible even with a single, three-component station. A single accelerogram available for the Erzincan, Turkey, 1992 March 13, $M_s = 6.8$ earthquake is inverted and the solution found is compatible with other seismological studies and with the mechanism expected for the North Anatolian Fault.

Key words: earthquake source mechanism, Erzincan earthquake, fault plane solutions, seismograms, strong ground motion, waveform analysis.

INTRODUCTION

The point source approximation is the basic element generally used for the inversion of seismic sources. In this case, it is not possible to identify the actual fault plane from the two nodal planes by using waveform modelling. For example, automatic determinations of focal mechanisms for teleseismic or regional events (e.g. Buland & Gilbert 1976; Dziewonski *et al.* 1981; Sipkin 1982, Dreger & Helmberger 1993; Kawakatsu 1995) give the seismic moment tensor, but cannot specify the actual fault plane. In order to select the actual fault plane, additional information such as the distribution of aftershocks or surface ruptures is needed. The approximation of a point source is generally valid for distances much larger than the size of the fault and the wavelength considered. However, at shorter distances this approximation is no longer appropriate, and the finiteness of the source should be taken into account. The problem of identification of the actual fault plane with a finite source model by waveform inversion has already been considered in several studies (e.g. Mori & Hartzell 1990; Dreger 1997), but in these works the focal mechanism is fixed in advance. Here, we show that the use a finite-dimension source model (FDSM hereafter) offers the possibility of determining the actual fault plane with little *a priori* information about the focal mechanism, even with data from a single station.

Accelerographs are well adapted to recording the dynamic and static parts of strong ground motions. However, many seismic regions of the world have only sparse strong motion networks. Hence, it is important to develop methods to identify the fault plane with one or few stations, especially when no precise aftershock locations or surface rupture is available. Accelerograms are often used in source studies for their high-frequency content (e.g. Spudich & Frazer 1984; Fletcher & Spudich 1998) but are used more rarely for their very low-frequency content and/or their static part (e.g. Legrand 1995; Delouis *et al.* 1997; Singh *et al.* 1997; Courboulex *et al.* 1997). The high-frequency part is usually thought to contain information about the complexity of the structure and the dynamics of the rupture: it will not be considered in this paper. We will model only the low-frequency parts of the signals, which contain information about the fault orientation and the slip direction.

DESCRIPTION OF THE POINT SOURCE AND FINITE-DIMENSION SOURCE MODELS

A physical finite-dimension fault of surface S over which surface forces are applied, generating a dislocation of value D, is mathematically equivalent, in the far field, to a point source where two couples of volume forces are applied, each of momentum $M_0 = \mu SD$ (Aki & Richards 1980), where μ is the shear modulus. However, when the source dimension is large enough relative to the hypocentral distance and to the wavelength, the source finiteness will have a strong effect on the shape of the seismograms (Fig. 1), and must be taken into account.

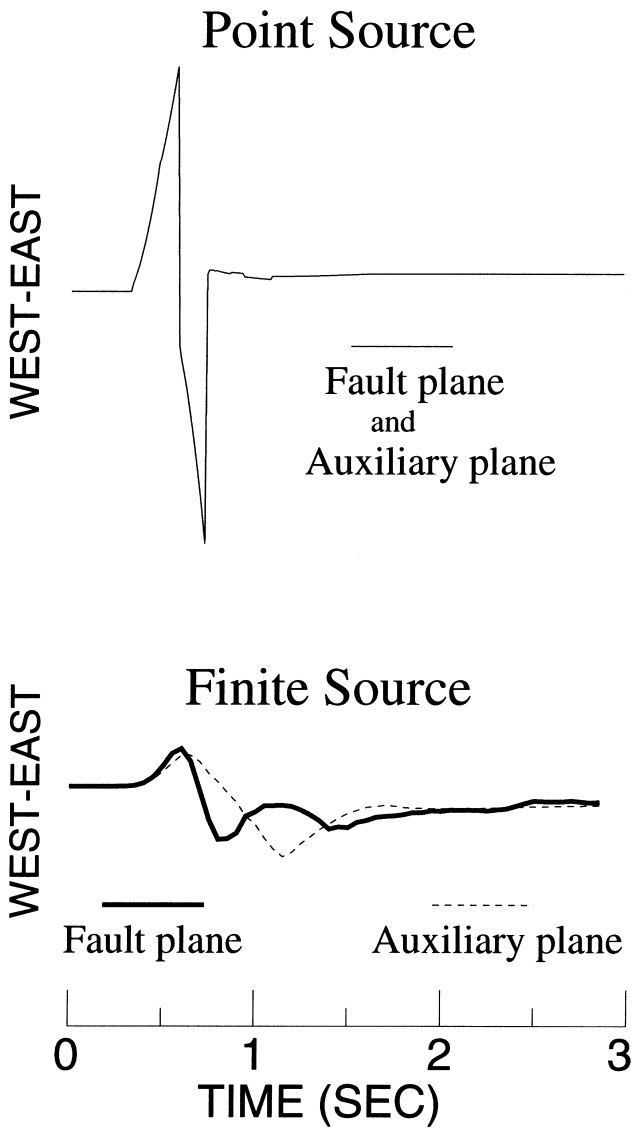

Figure 1. Comparison of a seismogram for a point source (top) an a finite-dimension source model (bottom). The fault plane is (strike, dip, rake)=(200, 70, 130) and the auxiliary plane is (312, 44, 29). The hypocentre is at 2 km depth and the epicentral distance is 1 km. For the FDSM, the nucleation point is at the centre of a 3 km × 3 km fault, the rupture front is circular and the constant rupture velocity is 2.5 km s^{-1}. The rise time is 0.15 s.

For a point source situated at $\xi = 0$, the displacement $u_n(\mathbf{x}, t)$ calculated at $\mathbf{x}$ and at time t is given by the representation theorem (Burridge & Knopoff 1964; Aki & Richards 1980),

$$u_n(\mathbf{x}, t) = \int_{-\infty}^{\infty} d\tau M_{ij}(0, \tau) g_{ni,j}(0, \tau; \mathbf{x}, t), \quad (1)$$

where g_{ni} is the Green's function tensor corresponding to a displacement in the n direction due to a unit force in the i direction and $g_{ni,j}(0, \tau; \mathbf{x}, t) = [\partial g_{ni}(\xi = 0, \tau; \mathbf{x}, t)]/\partial \xi_j$ are the spatial derivatives with respect to the source coordinates ξ.

For a point source at $\xi = 0$, the seismic moment tensor can be written as:

$$M_{ij}(0, \tau) = M_{ij} f(\tau),$$

where $M_{ij} = M_{ij}(\xi = 0)$ is the seismic moment tensor at the point $\xi = 0$ and f is the source time function. In that case (1) becomes

$$u_n(\mathbf{x}, t) = M_{ij} \int_{-\infty}^{\infty} d\tau f(\tau) g_{ni,j}(0, \tau; \mathbf{x}, t). \quad (2)$$

The source time function f used in this paper is a ramp function. The duration of the ramp corresponds to the rise time, T, and the final constant value, D, corresponds to the final static displacement on the fault plane (i.e. the dislocation D).

In the case of an FDSM, (1) becomes

$$u_n(\mathbf{x}, t) = \int_{-\infty}^{\infty} d\tau \iint_S d\xi_1 d\xi_2 M_{ij}(\xi, \tau) g_{ni,j}(\xi, \tau; \mathbf{x}, t), \quad (3)$$

where $\xi = (\xi_1, \xi_2)$ is the vector position describing the fault surface S.

In this paper, we will consider the simple case where the source time function f is the same at each point of the fault. Thus, we separate the spatial and temporal aspects of the source. With this simple assumption, (3) becomes

$$u_n(\mathbf{x}, t) = M_{ij} \int_{-\infty}^{\infty} d\tau f(\tau) \iint_S d\xi_1 d\xi_2 g_{ni,j}(\xi, \tau; \mathbf{x}, t). \quad (4)$$

Eqs (2) and (4) differ in the integration over the fault plane of surface S, and we show in this paper that this difference allows the selection of the fault plane if (4) is used instead of (2). Some caution is warranted in computing eq. (4). It is a joint integration in space and time which is approximated by a discrete summation of N point sources. As a consequence, the temporal and spatial sampling rates cannot be chosen independently (see the Appendix).

For the sake of simplicity, in this paper 'near field' (NF) means simply that the amplitude of NF waves are not negligible with respect to the amplitude of the far-field waves for the wavelength considered. As mentioned by Vidale *et al.* (1995) and Cummins (1997), NF waves can be clearly seen in some cases at teleseismic distances (20°–30°) for large earthquakes.

DISCRIMINATION OF THE FAULT PLANE FOR A FINITE-DIMENSION SOURCE MODEL WITH A SINGLE STATION

In the case of a point source, M_{ij} and the spatial derivatives of the Green's functions, $g_{ni,j}$, with respect to the source coordinates are the same, independent of which of the two nodal planes is the fault plane. The unique path of the $g_{ni,j}$ in that case is illustrated in Fig. 2(a). Hence, the seismograms corresponding to the two nodal planes will be identical (Fig. 1, top).

In the case of an FDSM, M_{ij} is also the same for the two nodal planes, but now $g_{ni,j}$ are different. In eq. (4), $g_{ni,j}$ correspond to the spatial derivatives of the Green's functions for all the paths between the surface S and the station considered. Since the orientations of the actual fault plane and the auxiliary plane are different, the corresponding paths of $g_{ni,j}$ differ, as shown in Figs 2(b) and (c). Consequently, the seismograms corresponding to the actual fault plane and the auxiliary plane will be different (Fig. 1, bottom). This difference in the waveforms of the seismograms will allow for the selection of the actual fault plane, as shown below.

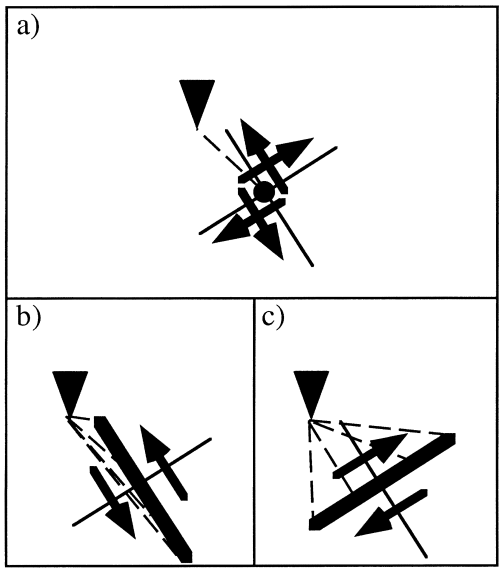

Figure 2. Scheme showing the different paths of the Green's functions (dashed lines) from the source to the station (triangle) for a point source model (a) and an FDSM (b and c). (a) The unique paths of the Green's functions for a point source (bold point) does not allow one to distinguish the fault plane from the auxiliary plane (the two lines). (b), (c) The different paths from the different points of the fault plane to the receiver allow one to discriminate the fault plane (bold line in b) from the auxiliary plane (bold line in c).

METHOD OF INVERSION

We invert NF records using a single three-component accelerogram using two models: a point source model and an FDSM. The spatial derivatives $g_{ni,j}$ of the Green's functions are calculated at the surface of a half-space using Johnson's (1974) method, which is based on Cagniard–de Hoop integration in the time domain. This calculation gives an exact analytic representation of the complete displacement field, including NF waves. In the case of an FDSM, some parameters (the dimension of the fault, the dislocation, the rise time and the rupture velocity) are fixed *a priori*, because with a single station these parameters cannot be constrained. We use a circular rupture front with a constant velocity and a constant dislocation over a rectangular fault. We took a nucleation point at the centre of the fault. The influence of the position of the hypocentre, controlling part of the history of the rupture, is important for modelling large earthquakes, but will not be considered here. The influence of the position of the nucleation point is discussed in more detail in Delouis & Legrand (1999).

We perform waveform modelling of body and surface waves in the time domain using a Monte Carlo inversion in order to find the orientation of the fault plane (strike and dip) and the direction of the slip vector on this fault (rake). The selection criterion in the Monte Carlo inversion is the normalized rms error (hereafter simply called rms) between the observed data (recorded seismograms) and the calculated synthetics. A first series of trials is performed for the entire space of solutions, and several subseries are made around the best solutions of the first series (zoom effect) to define the minimum, better. In order to find out whether we can select the fault plane from the two nodal planes, when a zoom is performed around a solution, we systematically carry out a second zoom around the corresponding auxiliary plane.

FIRST SYNTHETIC TEST

We apply the method with a point source model and with an FDSM for a first synthetic example, where the focal mechanism is fixed to (strike, dip, rake) = (200°, 70°, 130°). We calculate the corresponding three-component seismograms, called the 'synthetic data', which simulate observed data. These 'synthetic data' are inverted with the Monte Carlo approach described above, without adding any noise to the seismograms.

The 'synthetic data' that we invert are shown for a point source and for an FDSM in Fig. 1 for the fault plane (strike, dip, rake) = (200°, 70°, 130°) and the auxiliary plane (strike, dip, rake) = (312°, 44°, 29°). In this figure, we only show the E–W component for the sake of simplicity.

The results of the inversion of the synthetic data are shown for the point source and for the FDSM in Fig. 3. In both cases, the original focal mechanism is retrieved. In the case of a point source, the rms values are equal for the two nodal planes, hence they cannot be distinguished. This is expected since, as indicated above, the seismograms corresponding to the two

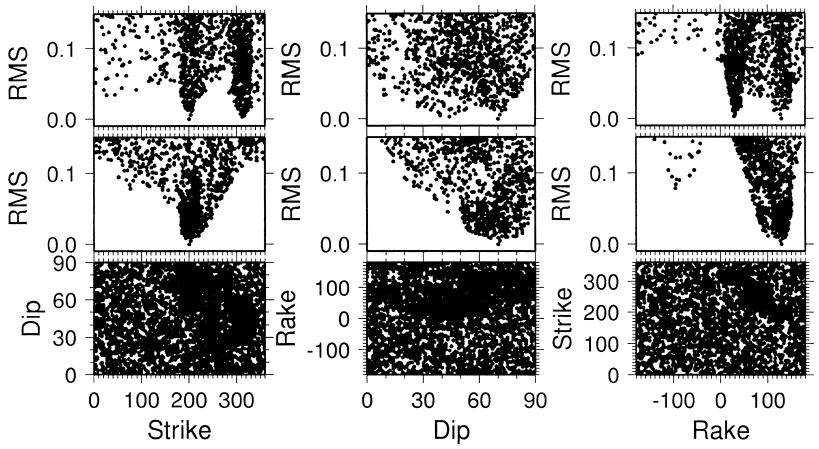

Figure 3. Rms results corresponding to the inversions for the first synthetic test. (Top) For a point source. The two nodal plane cannot be distinguished. (Middle) For an FDSM. The fault plane (strike, dip, rake) = (200°, 70°, 130°) can be distinguished from the auxiliary plane (strike, dip, rake) = (312°, 44°, 29°). (Bottom) Representation of all the 6181 sorts made by the Monte Carlo method.

nodal planes are identical. However, in the case of the FDSM, the rms values corresponding to the two nodal planes are significantly different, thus the fault plane can be clearly distinguished from the auxiliary plane, which has been rejected by the inversion. This is due to the difference in the corresponding seismograms. The results of the inversions are given in Table 1. The error estimates correspond to solutions having an rms within 10 per cent of the best rms found.

APPLICATION TO THE ERZINCAN (TURKEY) EARTHQUAKE: SECOND SYNTHETIC TEST AND INVERSION OF REAL DATA

The Erzincan earthquake (1992 March 13, $M_s = 6.8$) occurred along the North Anatolian Fault (Fuenzalida *et al.* 1997). The main shock was recorded by a single SMA-1 accelerograph located at an epicentral distance of about 10 km. Trial-and-error modelling of the seismograms, integrated from accelerograms, has been carried out by Legrand (1995) and Bernard *et al.* (1997). Legrand (1995) modelled the three components to determine the focal mechanism by trial and error, followed by a systematic search around the best solution using a simple model of propagation. Bernard *et al.* (1997) modelled the two horizontal components, taking into account the basin structure, with a fixed focal mechanism. In this paper we invert the same single three-component seismogram, as a test case for the method described above, focusing on the selection of the fault plane.

The medium of propagation used is a half-space, with $V_P = 6.0$ km s^{-1} and $V_S = 3.5$ km s^{-1}. The size of the fault has been taken as 25 km × 10 km, in accordance with the aftershock distribution and the magnitude. The rise time is 0.7 s and the rupture velocity is $V_r = 3$ km s^{-1} (Legrand 1995). We assume a circular rupture front, initiating at the centre of the fault. In the case of Erzincan, the number of trials (5381) in the Monte Carlo inversion is smaller than the 6181 trials for the synthetic case of Fig. 3 because the calculation of synthetic seismograms is time-consuming for such a large source. Hence, the uniqueness of the solution is not studied so completely.

This earthquake is a vertical strike-slip fault. In such a case, there is an ambiguity of $\pm 180°$ in both strike and rake. This means that the solution (strike, dip, rake) = (120°, 85°, −180°) and its auxiliary plane (210°, 90°, 5°) are almost the same as that with fault plane (300°, 85°, −180°) and auxiliary plane (30°, 90°, 5°). We carry out a second synthetic test to evaluate the resolution of the method described above for this particular situation. We construct the 'synthetic data' with a focal mechanism (strike, dip, rake) = (120°, 85°, −180°) close to the actual solution of the Erzincan earthquake. The first row of Fig. 4 shows the result of the inversion for a point source; four solutions can explain the 'synthetic data', which are the four triplets (strike, dip, rake) mentioned above. The second row of Fig. 4 also shows the solution for an FDSM; now only two solutions can explain the 'synthetic data', corresponding to the two triplets (strike, dip, rake) = (120°, 85°, −180°) and (300°, 85°, −180°) mentioned above. Finally, the third and fourth rows of Fig. 4 show the solution for the Erzincan earthquake for a point source and an FDSM, respectively. As for the synthetic test, it is not possible to identify the fault plane with a point source model, whereas it is possible to select the fault plane from the two nodal planes with an FDSM, because the two possible solutions found do not correspond to the classical indeterminacy between the two nodal planes, but to the ambiguity of $\pm 180°$ in both strike and rake mentioned above. The best solution corresponding to an FDSM is (124°, 90°, −172°) ± (2°, 1°, 3°), which is almost the same fault plane as the second minimum found (306°, 86°, 171°) ± (2°, 3°, 2°). These solutions are compatible with the right-lateral strike-slip mechanism of the North Anatolian Fault (Fuenzalida *et al.* 1997; Bernard *et al.* 1997). Hence, in the case of the Erzincan earthquake the correct fault plane has been automatically selected. The details of the solutions are given in Table 1.

Table 1. Errors are calculated from the standard deviation of the data with an rms smaller than the smallest rms + 10 per cent of the smallest rms. Note that the focal mechanism (120°, 85°, ±180°) is almost the same as (300°, 85°, ±180°); see text. The corresponding auxiliary planes are (210°, 90°, 5°) and (30°, 90°, 5°), respectively. FDSM = finite-dimension source model. All values are in degrees.

Focal mechanism (Input)	Best solutions (strike, dip rake)	Data type	Model
(200, 70, 130) = (312, 44, 29)	(203.0, 70.3, 127.6) ± (10, 5, 15) and (314.4, 44.0, 31.9) ± (11, 11, 7)	Synthetics	Point Source
(200, 70, 130)	(205.0, 66.6, 123.7) ± (11, 7, 13)	Synthetics	FDSM
(120, 85, −180) = (210, 90, 5)	(118.3, 82.2, 175.3) ± (4, 4, 3) (213.3, 86.2, 5.3) ± (4, 2, 3) (304.8, 86.6, 175.2) ± (3, 2, 3) (31.5, 83.2, 4.6) ± (4, 4, 3)	Synthetics	Point Source
(120, 85, −180)	(118.3, 83, 175.4) ± (3, 4, 3) (306.0, 87.1, 173.6) ± (2, 2, 2)	Synthetics	FDSM
	(120.0, 71.0, 175.0) ± (5, 10, 3) 210.0, 85.0, 7.0) ± (5, 3, 4) (304.0, 79.0, 174.0) ± (4, 7, 3) (33.0, 75.0, 9) ± (5, 4, 6)	Real data (Turkey)	Point source
	(124.0, 90.0, −172.0) ± (2, 1, 3) (306.0, 86.0, 171.0) ± (2, 3, 2)	Real data (Turkey)	FDSM

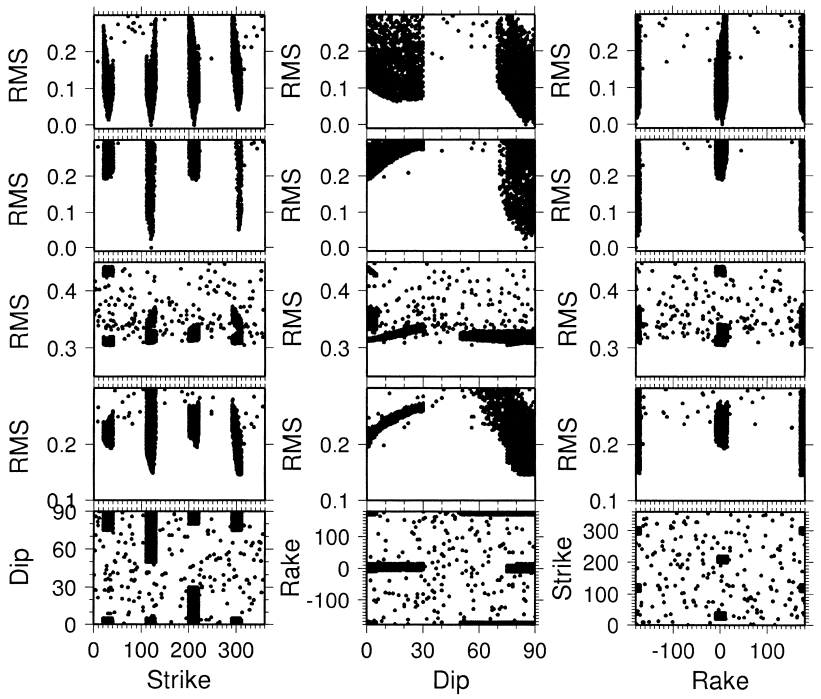

Figure 4. Rms errors for the second synthetic test for a point source model (first row) and an FDSM (second row) for a focal mechanism (strike, dip, rake) = (120°, 85°, −180°). The third and fourth rows correspond to the real Erzincan earthquake data for a point source and an FDSM, respectively. The last row corresponds to the sorts of Monte Carlo methods. A time shift of 0.12 s has been applied on the east component of the Erzincan data because of shear wave splitting observed on the data attributed to anisotropy (Bernard *et al.* 1997).

The seismograms corresponding to the best results are shown in Fig. 5 for a point source and an FDSM. The dislocation found is 1.5 m, corresponding to a seismic moment of 1.12×10^{26} dyn cm for a shear modulus of 3×10^{11} dyn cm^{-2}.

DISCUSSION

NF waves are often omitted in the calculation of synthetic seismograms. However, their contribution can be important in the case of a point source (see the NF ramp between the *P* and *S* pulses in Fig. 6, top), and extremely important in the case of a finite-dimension source (Fig. 6, bottom). Note that NF waves often appear as a ramp for a point source, whereas they often appear as a broad, low-frequency signal for a finite source.

NF waves decay as $1/r^2$, whereas the far-field waves decay as $1/r$, where r is the radial distance from the source to the receiver. Hence, a small change in distance implies a larger change in amplitude of the NF waves than the far-field waves, and, as a consequence, NF waves provide a sharp constraint on the orientation of a finite fault. This property is discussed in more detail and has been used to constrain the location and the focal mechanism of volcanic tremors for a point source by Legrand *et al.* (1999).

The waveforms of a moderate-sized earthquake may be modelled in the NF with a point source approximation (e.g. Singh *et al.* 1997; Schwartz 1995; Fan & Wallace 1991). In this case, the rise time has to be adjusted to the width of the observed waveform pulses. This leads to a long rise time which measures the total rupture duration of the faulting. It is longer than the 'physical' rise time of a specific point on the fault. With a finite-dimension source model, a more realistic (i.e. smaller) local rise time can be used. The low frequencies of the calculated seismogram will be naturally generated by the spatial integration over the fault plane (see Fig. 6) and not by increasing the rise time artificially when a point source is used.

Although we showed that the recovery of the fault plane with a single station is feasible, we do not imply that it will be possible in all cases. We cannot exclude the fact that for some specific station–fault geometries the constraint on the fault parameter may degenerate.

The velocity seismogram of the Erzincan earthquake is surprisingly low frequency, which seems to indicate a relatively simple rupture. This justifies the use of a simple model of homogeneous slip. However, for very large earthquakes, the rupture may become very heterogeneous, and it should certainly be taken into account in order to model adequately the seismograms. Here, a certain degree of heterogeneity may be invoked to explain part of the misfit in the modelling of the second pulse of the Erzincan data. The effect of the Erzincan basin, which we did not take into account, should also explain the misfit of the second pulse. However, the method appears to be robust enough, in the sense that this misfit did not seem to introduce a significant bias in the estimation of the focal mechanism.

CONCLUSIONS

The actual fault plane can be determined, with little *a priori* information on the focal mechanism, by waveform modelling, even with a single station, if an FDSM is used instead of a

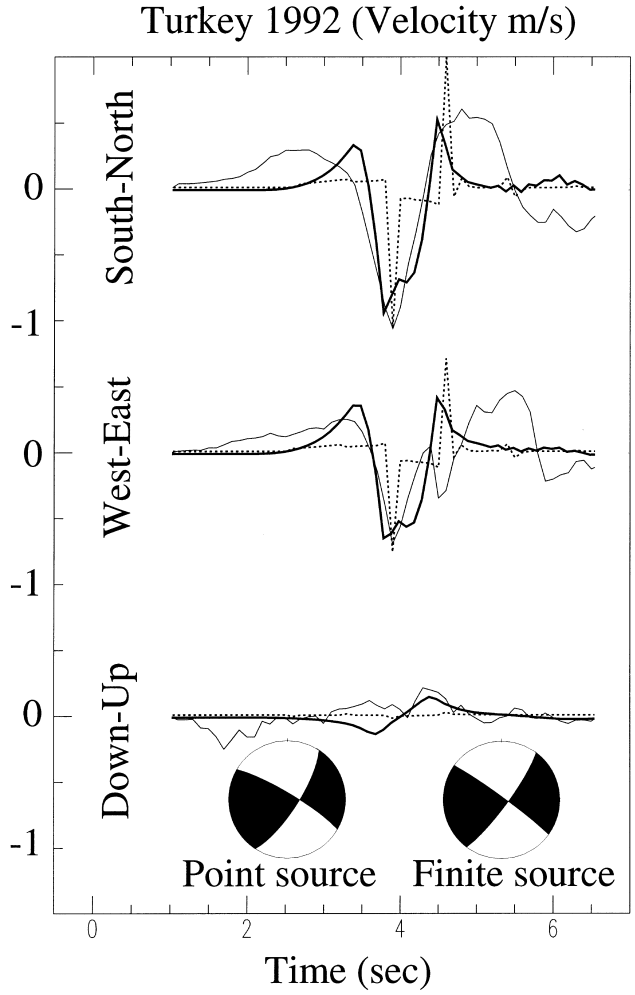

Figure 5. Result of the modelling of the three-component Erzincan seismogram (fine line) for a point source model (dotted line) and an FDSM (bold line), with the corresponding focal mechanism (lower-hemisphere, equal-area projection).

point source and if NF waves are taken into account in the calculation of Green's functions. With a single station, some of the source parameters such as the fault dimension, the rise time and the rupture velocity cannot be solved and have to be fixed *a priori* in the inversion. As a consequence, the knowledge of the source can be greatly improved not only by increasing the number of stations (as is often done) but also by considering FDSMs and using NF waves.

The method of selection of the fault plane from the two nodal planes described in this paper has been applied to local earthquakes but can be applied identically to regional and teleseismic events (especially for large earthquakes). This study points out the importance of low-frequency modelling in the NF. These low frequencies have two origins. First, NF waves are low frequency by nature. Second, the spatial and temporal finiteness of the source generate low frequencies. Hence, the use of accelerographs and/or broad-band stations in the NF is crucial for recording the static part and/or the low-frequency signal in order to constrain the fault plane orientation and the slip vector.

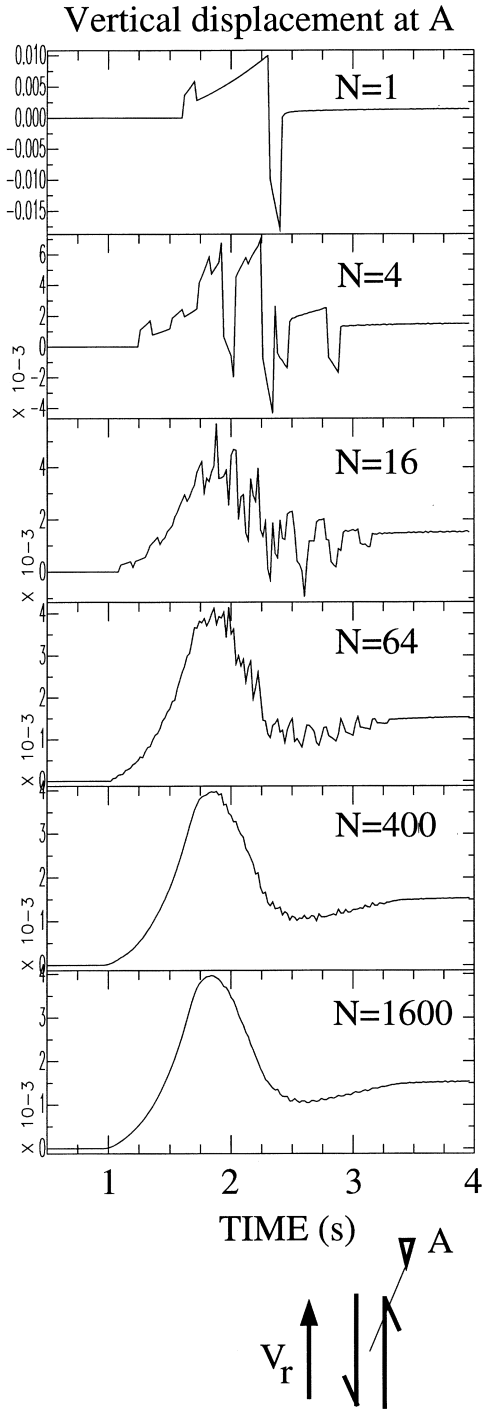

Figure 6. Vertical displacement for a pure strike-slip mechanism recorded at station A. The rupture propagates towards A. N is the number of point sources. An FDSM is well described by at least 400 point sources. See text for more details. The rupture front here is taken as linear and unilateral, in the sense shown by the arrow at the bottom of the figure, the rupture velocity being 3 km s^{-1}. The size of the fault is 4 km × 4 km and the coordinates of A are (3 km N, 0.1 km E); $\Delta t = 0.02$ s. Vertical scale in arbitrary units, depending on the value of the dislocation D, which is the same for all of this figure.

We have shown that in the case of the Erzincan (Turkey) earthquake, the fault plane can be distinguished from the two nodal planes with records from a single station when an FDSM and NF waves are used. The selected fault plane

corresponds to the orientation of the North Anatolian Fault, and the focal mechanism is right-lateral strike slip, as expected for the North Anatolian Fault.

ACKNOWLEDGMENTS

We would like to thank the French Ministère des Affaires Etrangères and ETH Zurich for their support, and Prof. Kawakatsu for his hospitality towards DL. We are grateful to two anonymous reviewers for their critical comments of the manuscript.

REFERENCES

Aki, K. & Richards, P., 1980. *Quantitative Seismology: Theory and Methods,* W. H. Freeman, New York.

Bernard, P., Gariel, J.C. & Dorbath, L., 1997. Fault location and rupture kinematics of the magnitude 6.8, 1992 Erzincan earthquake, Turkey, from strong ground motion and regional records, *Bull. seism. Soc. Am.,* **87,** 1230–1243.

Buland, R. & Gilbert, F., 1976. Matched filtering for the seismic moment tensor, *Geophys. Res. Lett.,* **3,** 205–206.

Burridge, R. & Knopoff, L., 1964. Body force equivalents for seismic dislocations, *Bull. seism. Soc. Am.,* **54,** 1875–1888.

Courboulex, F., Santoyo, M.A., Pacheco, J.F. & Singh, S.K., 1997. The 14 September 1995 (M = 7.3) Copala, Mexico, earthquake: a source study using teleseismic, regional, and local data, *Bull. seism. Soc. Am.,* **87,** 999–1010.

Cummins, P., 1997. Earthquake near-field and W phase observations at teleseismic distances, *Geophys. Res. Lett.,* **24,** 2857–2860.

Delouis, B. & Legrand, D., 1999. Focal mechanism determination and identification of the fault plane of earthquakes using only one or two near source seismic recordings, *Bull. seism. Soc. Am.,* submitted.

Delouis, B. *et al*., 1997. The Mw = 8.0 Antofagasta (Northern Chile) earthquake of 30 July 1995: a precursor to the end of the large 1877 gap, *Bull. seism. Soc. Am.,* **87,** 427–445.

Dreger, D., 1997. The large aftershocks of the Northridge earthquake and their relationship to mainsshock slip and fault-zone complexity, *Bull. seism. Soc. Am.,* **87,** 1259–1266.

Dreger, D. & Helmberger, D., 1993. Determination of source parameters at regional distances with single station or sparse network data, *J. geophys. Res.,* **98,** 8107–8125.

Dziewonski, A., Chou, T. & Woodhouse, J., 1981. Determination of earthquake source parameters from waveform data for studies of global and regional seismicity, *J. geophys. Res.,* **86,** 2825–2852.

Fan, G. & Wallace, T., 1991. The determination of source parameters for small earthquakes from a single, very broadband seismic station, *Geophys. Res. Lett.,* **18,** 1385–1388.

Fletcher, J. & Spudich, P., 1998. Rupture characteristics of the three M ~ 4.7 (1992–1994) Parkfield earthquakes, *J. geophys. Res.,* **103,** 835–854.

Fuenzalida, H. *et al*., 1997. Mechanism of the 1992 Erzincan earthquake and its aftershocks, tectonics of the Erzincan basin and decoupling on the North Anatolian Fault, *Geophys. J. Int.,* **129,** 1–28.

Hartzell, H., Frazier, G. & Brune, J., 1978. Earthquake modeling in a homogeneous half-space, *Bull. seism. Soc. Am.,* **68,** 301–316.

Johnson, L., 1974. Green's function for Lamb's problem, *Geophys. J. R. astr. Soc.,* **37,** 99–131.

Kawakatsu, H., 1995. Automated near-realtime CMT inversion, *Geophys, Res, Lett.,* **21,** 1963–1966.

Legrand, D., 1995. Study of a population of tectonic and volcanic earthquakes in near-field: from classical seismology to non linear effects, *PhD thesis,* University of Strasbourg (in French).

Legrand, D., Kaneshima, S. & Kawakatsu, H., 1999. Moment tensor analysis of near-field broadband waveforms at Aso volcano, Japan, *J. Volc. Geotherm. Res.,* in press.

Mori, J. & Hartzell, S., 1990. Source inversion of the 1988, Upland, California earthquake: determination of a fault plane for a small event, *Bull. seism. Soc. Am.,* **80,** 507–518.

Schwartz, S.Y., 1995. Source parameters of aftershocks of the 1991 Costa Rica and 1992 Cape Mendocino, California, earthquake from inversion of local amplitude ratios and broadband waveforms, *Bull. seism. Soc. Am.,* **85,** 1560–1575.

Singh, S.K., Pacheco, J., Courboulex, F. & Novelo D.A., 1997. Source parameters of the Pinotepa Nacional, Mexico, earthquake of 27 March, 1996 (Mw = 5.4) estimated from near-field recordings of a single station, *J. Seism.,* **1,** 39–45.

Sipkin, S., 1982. Estimation of earthquake source parameters by the inversion of waveform data: synthetic waveforms, *Phys. Earth planet. Inter.,* **30,** 242–259.

Spudich, P. & Frazer, L., 1984. Use of ray theory to calculate high-frequency radiation from earthquake sources having spatially variable rupture velocity and stress drop, *Bull. seism. Soc. Am.,* **9,** 2061–2082.

Vidale, J.E., Goes, S. & Richards, P.G., 1995. Near-field deformation seen on distant broadband seismograms, *Geophys. Res. Lett.,* **22,** 1–4.

APPENDIX A: PROBLEM OF THE SPATIO–TEMPORAL INTEGRATION ON A FAULT PLANE

A finite-dimension source can be modelled by a superposition of point sources located on the fault plane at $\boldsymbol{\xi} = (\xi_1, \xi_2)$, performing the continuous spatial integral (4) by a discrete spatial summation of N point sources. As the representation theorem deals with an integration in both time and space, the temporal and spatial samplings cannot be chosen independently, but must verify some conditions of sampling such as those described by Hartzell *et al.* (1978). The spatial sampling described by Hartzell, if applied as a limit, is in practice not small enough, so some artificial high frequencies are generated. We proceed empirically. First, the time sampling is chosen for a point source. It must be small enough to describe all the wavelengths considered in the seismogram and to sample the rise time correctly, but not too small, in order to avoid high-frequency noise of numerical origin. When the time sampling for a point source is chosen, the spatial sampling is determined as follows. It is reduced until the seismogram reaches a stable form. The spatial sampling must not be too large, otherwise high frequencies are generated due to the sampling rate condition described by Hartzell *et al.* (1978) not being respected, or too small, because in that case it is time-consuming and high frequencies due to numerical effects are also generated. This procedure is illustrated in Fig. 6, for which a finite-sized fault plane has been modelled with $N = 1$, 4, 16, 64, 400 and 1600 point sources. If too small a number of point sources is used in the summation, high frequencies arise (like for $N = 4$, 16, 64) due to the space–time samplings not being respected. We see that 400 point sources is almost enough to describe the finiteness of the source. Note the large difference between the signals from a point source and from a finite-dimension source. For a point source, positive and negative parts of the signal exist, whereas for a finite source, only a positive signal remains. A finite-dimension source contains many more low frequencies than a single point source. For example, the P and S waves which have a form similar to a Dirac distribution almost disappear in the case of a finite source; P and S waves cannot be distinguished for a finite-dimension source, whereas it is possible for a point source. These low frequencies are

partly generated by the constructive and destructive interference of waves, especially NF waves. It is a well-known fact that a large earthquake generates more low frequencies than a small earthquake. Note also that we focus on the effect of the finiteness in space introduced by the length and width of the fault, but a similar effect also exists in time, introduced by the rise time, which is the time taken for each point of the fault to reach the final dislocation D (the static displacement). For a point source, this rise time governs the width of the far-field P and S waves (see Fig. 6, for $N = 1$), whose forms are similar to Dirac pulses as mentioned above. Fig. 6 shows the effect of this rise time during the summation process.